Assessing the Impact on Power Production of WEC array separation distance in a wave farm using one-way coupling of a BEM solver and a wave propagation model

Philip Balitsky
Department of Civil Engineering, Ghent University
Technologiepark 904, B-9052, Ghent, Belgium
E-mail: philip.balitsky@ugent.be

Gael Verao Fernandez
Department of Civil Engineering, Ghent University
Technologiepark 904, B-9052, Ghent, Belgium
E-mail: gael.veraofernandez@ugent.be

Vasiliki Stratigaki
Department of Civil Engineering, Ghent University
Technologiepark 904, B-9052, Ghent, Belgium
E-mail: vasiliki.stratigaki@ugent.be

Peter Troch
Department of Civil Engineering, Ghent University
Technologiepark 904, B-9052, Ghent, Belgium
E-mail: peter.troch@ugent.be

***Abstract*—One of the key challenges in designing a Wave Energy Converter (WEC) farm is that the devices hydrodynamically interact with one another. Therefore their positioning will impact both the power output of a given wave energy project and any potential effects on the surrounding areas. The wave energy farm developer then must optimize the positioning of the devices to maximize power output whilst at the same time minimizing capital cost and any potential deleterious external effects. A number of recent studies have shown that one potential solution is that instead of spreading the devices uniformly, they can be placed in dense *clusters* or arrays of several devices with space available in between for navigation. In this paper we apply a novel one-way coupling method between the BEM model NEMOH and the wave propagation model MILDwave to investigate the influence on power output of the separation distance between two densely packed WEC arrays in a wave farm. An iterative method of applying the one-way coupling to interacting WEC arrays is used to compute the wave field in a WEC farm and to calculate its power output. The wave farm is modelled for regular waves for a number of wave periods, wave incidence directions and various inter-array separation distances. The notion of WEC array independence is defined and discussed for a 2-array WEC farm with a view towards simplifying the modelling calculations.**

***Index Terms*—hydrodynamic interactions, WEC array, WEC farm, separation distance, wave incidence angle, near-field effects, far-field effects, model coupling, BEM, mild-slope, MILDwave, NEMOH.**

NOMENCLATURE

β	angle of incidence of the incoming wave to the x-axis [°]
d_x, d_y	WEC separation distances in the x and y direction [m]
B_{PTO}	power-take-off damping coefficient [kg/s^2]
D_1	array centre-to-centre separation distance [m]
N	number of bodies in the WEC array
η	free surface elevation [m]
$\|\eta\|$	absolute value of the complex wave amplitude η [m]
p_ij	perturbed wave of order j for array i [-]
$P_i(\omega, \beta)$	mechanical power produced by the WEC [kW] for a given frequency and wave direction
r_c	coupling radius [m]
T_r	resonance or natural period of an oscillating body [s]
X_i	complex amplitude of heave velocity

perturbed wave = radiated+diffracted wave

I. INTRODUCTION

Ocean Wave Energy is a promising source of clean electricity that has the potential to make a significant contribution in reducing the world's dependence on fossil fuels. However, in order for it to follow the path of offshore wind and become a commercially viable power source, significant cost reductions must be made. Because of physical restrictions on the size of the individual devices, it is the established view of the wave energy industry that Wave Energy Converters (WECs) will have to be deployed in farms to be economically viable. To benefit from the developing offshore infrastructure and the maritime support industry, such farms will need to have a power rating on the order of hundreds of megawatts. With the most promising current WEC technology, this corresponds to WEC farms of hundreds of devices. How these WECs are grouped and arranged within a wave farm to maximize profitability whilst minimizing detrimental effects is still an open question. For a key group of WECs nearing commercial deployment, i.e. heaving axi-symmetric point absorbers, a number of recent studies have investigated numerically and experimentally the layout and spacing of devices within the

WEC array or farm [1]–[5]. Although the terms "WEC farm" and "WEC array" are used interchangeably, we will define a "WEC farm" as comparable in size to an offshore wind farm that may consist of a large number of sparsely separated WECs or clusters of densely packed WECs which we hereby term "WEC array". A large number of these investigations utilized potential flow theory, specifically the Boundary Element Method (BEM) to resolve the inter-array effects. While effective for arrays with a small number of bodies, BEM modelling becomes computationally demanding as the number of bodies and modelled frequencies increase. We follow an alternative approach whereby a WEC farm comprising two WEC arrays is modelled using a one-way coupling technique between the BEM model NEMOH [6] and a wave propagation model MILDwave [7], [8]. *One-way coupling* simply means that the information is propagated from the nested model to the outer model but not vice-versa. We use the BEM model in the *near-field* area of the WEC arrays and the wave propagation model in the *far-field* WEC farm area external to the WEC arrays (see Fig. 1). The latter domain also includes regions outside the WEC farm that are affected by it. A key

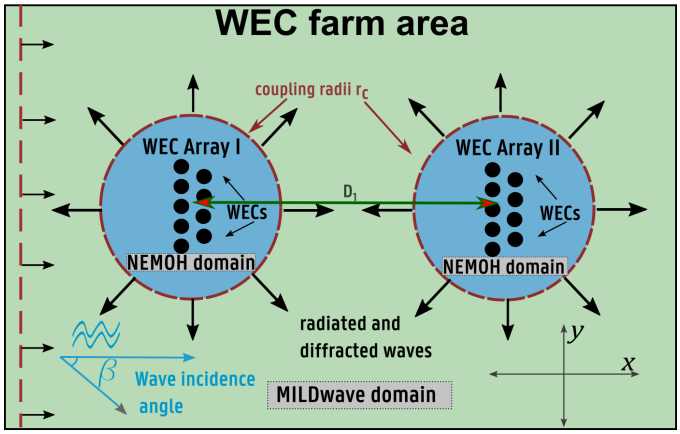

Fig. 1: SCHEMATIC OF THE CLUSTERED WAVE FARM LAYOUT

feature of the proposed one-way coupling technique is that waves are propagated from the near-field model (NEMOH) domain to the far-field model (MILDwave) domain via a transfer of information on a wave generation circle at the coupling radius r_c. A schematic of these domains and the clustered wave farm layout is presented in Fig. 1. The wave loading in NEMOH is determined by the wave conditions in the domain at the WEC array location. If the effect of one array on another is sufficiently small then these disturbances in the wave field due to the interaction can be ignored, and therefore the arrays can be simulated by the same incident wave conditions. If the WEC arrays are sufficiently close for mutual hydrodynamic interaction, however, the effect of the perturbed (radiated plus diffracted) waves from one array on another need to be taken into account. Such an approach would of course require multiple simulations and would take a longer time to perform. The crucial question then is at what distance can we consider two arrays to be sufficiently hydrodynamically independent to warrant a coupling approach where interaction is ignored. In this investigation, we aim to provide the answer to the above, namely, how much is the power output of a given WEC array affected by another WEC array for a given set of regular wave conditions and WEC farm layouts. Two staggered arrays of nine point absorber type heaving WECs are modelled using the aforementioned coupling hydrodynamically independent. Various array separation distances are simulated for a number of incident wave headings. The power output for the different configurations is calculated and compared to that of a farm of hydrodynamically independent WEC arrays, i.e. those operating in isolation. The minimum separation distance for which two WEC arrays in a farm can be considered as hydrodynamically independent is defined for each wave period. As our focus is on operational sea states, in this work we operate in the paradigm of linear potential theory, as detailed in Section II.

II. Theoretical Background

A. Linear Potential Flow

This investigation assumes linear potential flow theory [9], a subset of linear wave theory that allows the flow velocity, v, to be expressed as the gradient of the potential, Φ (Eq. (1)).

$$v = \nabla\Phi \tag{1}$$

The assumptions underlying potential flow are the following:

- The flow is inviscid;
- The flow is irrotational;
- The flow is incompressible.

The standard assumption of linear theory that the motion amplitudes of the bodies are much smaller than the wavelength also applies. Linear potential flow theory has hitherto been utilized in a majority of the investigations into WEC array modelling, for example see [3], [10], [11]. Due to the principle of superposition, linear potential theory allows for the separation of the total wave field into the following components (Eq. (2)):

$$\varphi_t(x,y,z) = \varphi_i + \varphi_d + \sum_i^6 \varphi_r \tag{2}$$

where φ_t is the total velocity potential, φ_i is the incident wave potential, φ_d the diffracted wave potential and $\sum_i^6 \varphi_r$ is the sum of the radiated wave potentials for each Degree of Freedom (DoF) of the device. In our investigation we only model the heave motion for simplicity and because heave is the primary operating DoF of the devices modelled. We also make use of the term perturbed wave to denote the wave resulting from sum of the diffracted and radiated potentials.

B. Boundary Element Method Solver

In our coupling approach the *inter-array* effects, induced by the hydrodynamic interaction between the devices, are

resolved by simulating the WEC motions using the open-source potential flow BEM solver NEMOH. Given Eq. (1), NEMOH solves the Laplace equation Eq. (3) for the complex velocity potential, φ:

$$\Delta\varphi = 0 \tag{3}$$

given a set of boundary conditions on the wetted body surface, the free surface, sea bottom and far-field. The equations of motion are solved using the method of Green's functions, as explained in [6]. An important restriction imposed by the method is the assumption that the water depth h is constant throughout the inter-array domain (NEMOH domain in Fig. 1). The free surface elevation η is calculated by taking the real part of the complex potential $\bar{\eta}$ that is in turn obtained in NEMOH from the free surface boundary condition Eq. ((4)). From the superposition principle of Eq. (2), free surface elevations η can be obtained separately for the WEC motions due to the diffracted and the radiated potentials.

$$\eta = -\frac{1}{g}\left(\frac{\partial\varphi}{\partial t}\right)_{z=0} \tag{4}$$

where g is the acceleration due to gravity and z is the vertical water velocity.

C. Mild-slope Wave Propagation Model

For simulating the far-field effects, e.g. the shadow zone of the area of the 'wake effects' in lee of the array, the wave propagation model MILDwave is employed [7], [8]. MILDwave, developed at the Coastal Engineering Research Group of Ghent University, Belgium, is a phase-resolving model based on the depth-integrated mild-slope equations (Eqs. (5a) and (5b)) introduced by Radder and Dingemans [12]. This particular model has been used in modelling WEC arrays in a number of recent publications [1], [8], [13]–[15]. The mild-slope equations (Eqs. (5a) and (5b)) are solved using a finite difference scheme that consists of a two-step space-centred, time-staggered computational grid, as detailed in [16].

$$\frac{\partial\eta}{\partial t} = \frac{\omega^2 - k^2 C C_g}{g}\varphi - \nabla\cdot\left(\frac{CC_g}{g}\nabla\varphi\right) \tag{5a}$$

$$\frac{\partial\varphi}{\partial t} = -g\eta \tag{5b}$$

Here η and φ_t are, respectively, the surface elevation and the total velocity potential at the free water surface, g is the gravitational acceleration, C is the phase velocity and C_g the group velocity for a wave with wave number k and angular frequency ω.

III. Coupling Methodology

A. Modelled WECs

The type of WECs modelled in this study is a flat circular cylinder with a diameter of 10 m and a draft of 2 m. The shape was selected based on its overall dimensions being similar to several promising WEC technologies, namely those of Seabased, Seatricity and Carnegie Wave [17]. All three devices are in the planning stages of a pre-commercial WEC array. The Power Take-Off (PTO) of each WEC is modelled as a resistive damper with a B_{PTO} value of $3.6 \times 10^5 kgs^{-2}$, which is representative for a resistive PTO of the WEC type we model [18]. The natural or resonance period of the device, T_r, is equal to 4.6 s and the value of B_{PTO} is set constant for each of the WECs in an array. Further details can be found in [15].

B. WEC Array and WEC Farm Layout

To simulate a realistic array of WECs, we have chosen a staggered configuration that has been shown in [19], [20] to maximize power in both equal and irregular sea states. For each of the farm configurations, we simulate two 9-WEC arrays as shown in Fig. 2 within the farm shown in Fig. 1 at various distances D_1 from each other. The array orientation is held constant while the angle of the incoming waves relative to the x-axis, β, is set at $0°$, $45°$, and $90°$. A schematic of the farm layout is shown in Fig. 1. In this investigation the water depth is held constant at 40 m.

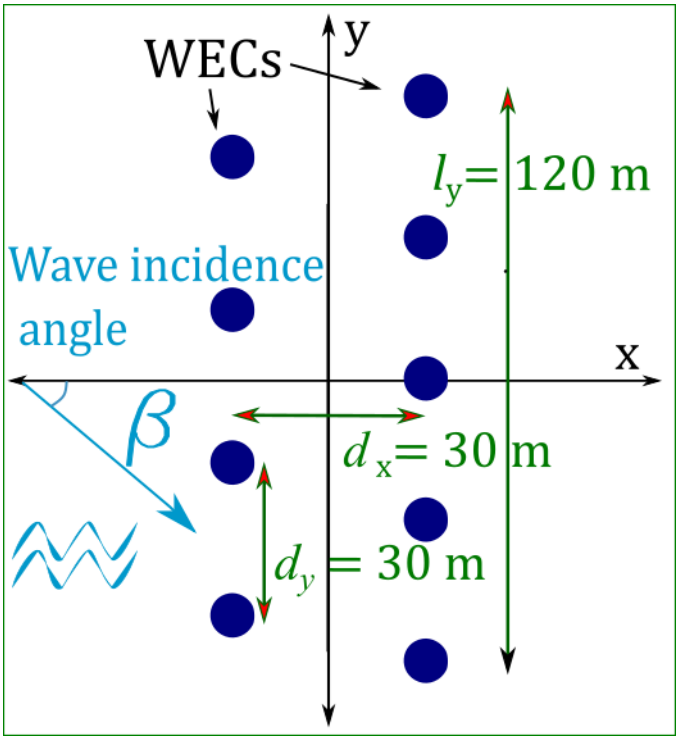

Fig. 2: PLAN VIEW OF THE ARRAY LAYOUT FOR TWO AND THREE BUOYS. THE INCIDENT WAVE MAKES DIRECTION β WITH THE x-AXIS

C. Coupling of NEMOH to MILDwave

In order to model the far-field effects in an efficient manner with a reasonable accuracy, a one-way coupling methodology introduced in [13], [15] is employed. In brief, the perturbed wave field is calculated in the BEM code NEMOH and is propagated into the depth-integrated wave model MILDwave on a circle large enough to enclose the near-field domain that

contains the WECs. Based on the aforementioned analysis, we set the coupling radius r_c at the smallest possible value which results in a discrepancy of less than 2 % in $|\eta|$ between NEMOH and MILDwave. For this investigation the value of r_c is set at 100 m. The MILDwave gird resolution is set at Δx = Δy = 2 m. For further details on the coupling are available in [15].

D. Calculating the Total Wave Field of the Perturbed Sea State

To assess the effects of the two WEC arrays within a WEC farm on each other, and in order to evaluate the power output of the farm, we need to calculate the total perturbed wave field in the MILDwave domain. As we assume linear theory in our work, we can use the superposition principle to sum up the total wave field by combining an iterative approach with the coupling methodology presented in Section III-C. The technique employed is illustrated in Fig. 3. The initial step (Step 1) is to propagate the incident wave in the empty numerical basin to obtain the undisturbed wave elevation. In Step 2 the incident wave elevation is used as input into NEMOH whence the 1st order perturbed wave of WEC Array I, p_{1i}, is evaluated. In Step 3, the average wave amplitude at the location of p_{1i} is used as input into NEMOH to calculate the 1st order perturbed wave of WEC Array II, p_{1ii}. In Step 4, the process in Step 2 is repeated, with p_{1ii} as the new input perturbed wave. Finally in Step 5, the same process is performed for the 2nd perturbed wave of WEC Array I, p_{2i}. Since the input perturbed wave in each subsequent step after step is reduced by approximately an order of magnitude, for all practical purposes this process can be terminated at Step 4 without any appreciable loss in accuracy, even for the case where interaction is maximized. Therefore, Step 5 is only displayed for a complete description of the proposed coupling methodology.

E. Determining the Power Output of a 9-WEC Array

To demonstrate the influence of the WEC array-WEC array interaction effects on the performance of a wave farm, we compute the total power produced by the two WEC arrays, after having obtained the modified wave field using the approach outlined in Section III-D. For each WEC array, using the amplitude of the total wave field at the locations of the WECs as the input, we calculate the power output in NEMOH for each WEC in the array using Eq. (6). The total power output of the wave farm is the sum of the power produced by the two WEC arrays. For a WEC in regular waves, the mechanical power output P extracted at each frequency ω and incidence angle β for a unit of wave amplitude is:

$$P_i(\omega,\beta) = \frac{1}{2}\sum_{i=1}^{N} \mathbf{B}_{PTO}\omega^2 |X_i(\omega,\beta)|^2 \qquad (6)$$

where N is the number of bodies in the array, X_i is the complex velocity in heave of each WEC body, and B_{PTO} is the PTO damping coefficient which in our case is a equal to $3.6 \times 10^5 kgs^{-2}$ for each WEC. While this method does not achieve the optimal power that would be produced by a fully reactive system, the scenario does represent an array with a realistic motion for the specific shape of the devices investigated.

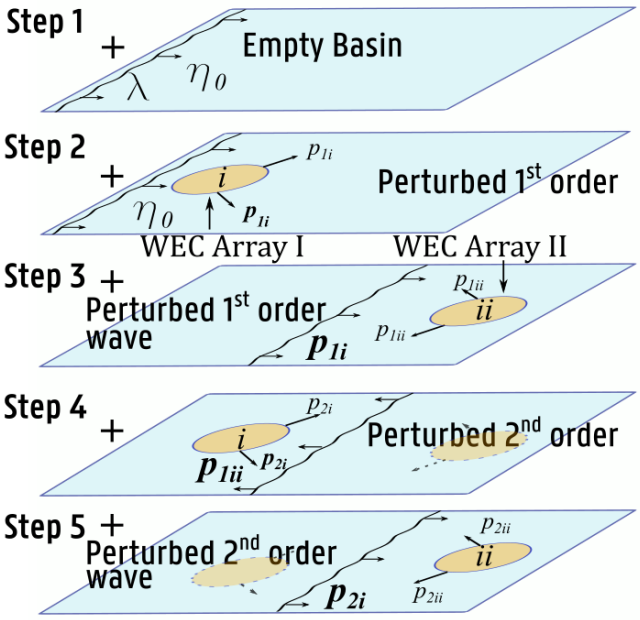

Fig. 3: TECHNIQUE FOR DETERMINING THE PERTURBED FIELD FOR A REGULAR INPUT WAVE. THE PROPOSED TECHNIQUE IS BASED ON THE PRESENTED STEP-BY-STEP PROCEDURE. THE INCIDENT WAVE IS PROPAGATING FROM THE LEFT.

IV. RESULTS

A. Wave Field Around two WEC Arrays within a WEC Farm

Before moving on to investigate the power output of each WEC array at various separation distances, we show an example of the perturbed wave field around two WEC arrays. To do so, we use the technique outlined in Section III-D to elaborate on the characteristics of the wave field in the presence of the two WEC arrays. The presented results refer to the minimum and maximum distance modelled, that is a separation distance equal to $2r_c$ and $5r_c$, respectively, for a regular wave of wave periods T = 6 s, T = 8 s, and T = 10 s. This is equivalent to D_1 = 200 m and 600 m, respectively. The results for T = 6 s are shown in (a) and (b) in Fig. 4, while while those for T = 10 s are displayed in (c) and (d) in Fig. 4. Note that the wave field shown inside the r_c of both WEC arrays is the wave field calculated in NEMOH initialized by the average $|\eta|$ given by MILDwave at the end of Step 4 as shown in Fig. 3 in Section III-D. In the top row in Fig. 4 we observe that the wave field around the arrays is strongly modified, with significant interaction patterns, especially in front of the WEC arrays. For the minimum separation distance,

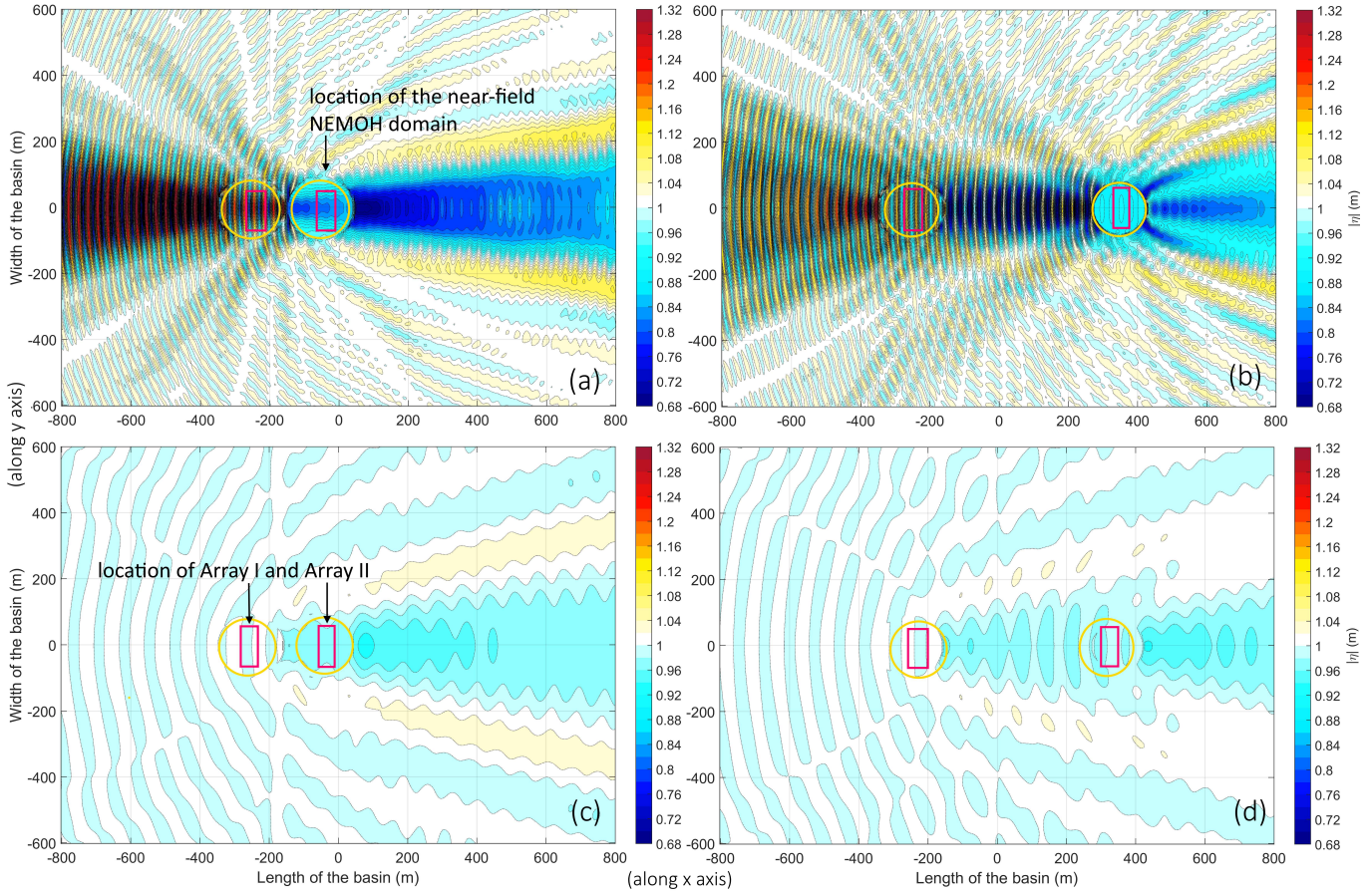

Fig. 4: WAVE FIELD AROUND TWO WEC ARRAYS, I (LEFT) AND II (RIGHT), OF 9 HEAVING BUOYS FOR REGULAR WAVES OF T = 6 s (TOP ROW) AND T = 10 s (BOTTOM ROW). WEC ARRAY SEPARATION DISTANCE D_1 = 200 m or $2r_c$ (LEFT COLUMN) AND D_1 = 600 m or $6r_c$ (RIGHT COLUMN)

that is D_1 = 200 m, the *far-field* effects of the two WEC arrays overlap and enhance each other. We see a significant decrease of the wave amplitude behind the arrays and a large area of mostly positive anomalies at the front. When we increase the separation distance we see an even more complicated pattern of the two WEC arrays' perturbed waves interacting in the area between the WEC arrays. Note, however, that the *wake effect*, that is the area of reduced $|\eta|$ downwave of the WEC array, is strongly positive while the energy in front of the first WEC array is strongly enhanced. The result is that the total power of a farm of WEC arrays aligned to the angle of wave propagation will highly depend on the distance between the WEC arrays, something which we will observe in Section IV-B. For T = 10 s the pattern is similar to the previous two cases, albeit with a significant decrease in the overall magnitude of the interaction effects such that they can be ignored, which shall be explored in more detail in Section V. In brief, given all the assumptions characteristic of linear theory and the simplifications of the buoy shape and PTO model, the 4% maximum difference shown between the incident wave and the perturbed wave is well within the margin of error. In this particular case then, the WEC array separation distance will in practise be driven by factors other than hydrodynamic interactions between the two WEC arrays.

B. Power Output of a WEC farm Composed of 2 WEC Arrays

In the next two subsections we will expand on the qualitative observations made in Section IV-A, by quantifying the power output by a WEC farm composed of two WEC arrays separated by a distance D_1 for incident waves of T = 6 s, T = 8 s, and T = 10 s. The waves simulate propagate from three different incidence angles β, i.e. $0°$, $22.5°$, and $45°$. The method outlined in Section III-E is employed to calculate the power output of the 2-Array WEC farm for a range of separation distances. P_I and P_{II} is the power output of WEC Array I and of WEC Array II, respectively. The results are displayed for each period in Table I with the power of each WEC array calculated separately, then summed together for the total power output of the entire wave farm. Note that the power of the hydrodynamically independent 9-WEC array operating in isolation, is displayed in column 4 ($D_1 = \infty$). We first note the overall trend in the power output, with the wave at T = 6 producing the most power with decreasing values for T =

TABLE I: TOTAL POWER (kW) OUTPUT OF A TWO 9-WEC ARRAY WAVE FARM FOR: WAVE PERIODS OF T = 6 s, T = 8 s AND T = 10 s, FOR A RANGE OF CENTRE-TO-CENTRE ARRAY SEPARATION DISTANCES, D_1, AND FOR DIFFERENT WAVE INCIDENCE ANGLES, β

wave period T (s)	wave inc. angle β (°)	output power (kW)	Separation distance, D_1, between WEC Array I and WEC Array II (m)										
			∞	200	300	400	500	600	700	800	900	1000	1200
6	0	P_I	$P_{arr} =$	1310.09	944.16	1541.24	668.12	1648.30	681.15	915.50	915.50	1252.07	940.18
		P_{II}	1111.04	695.80	1054.22	687.80	969.34	746.61	903.24	855.45	855.45	949.57	963.70
		P_{farm}	2222.07	2005.88	1998.38	2229.04	1637.46	2394.91	1584.40	1770.95	1770.95	2201.64	1903.88
	22.5	P_I	$P_{arr} =$	860.44	904.63	1077.71	848.99	1029.17	1029.17	959.59	959.59	919.74	918.62
		P_{II}	947.90	950.16	966.81	1032.00	995.16	971.96	971.96	922.15	919.74	937.73	959.39
		P_{farm}	1895.80	1810.60	1871.44	2109.71	1844.15	2001.12	2001.12	1881.74	1879.33	1857.46	1878.01
	45	P_I	$P_{arr} =$	599.48	583.97	590.10	584.34	587.68	587.68	586.63	658.35	586.45	584.98
		P_{II}	578.14	587.76	845.63	746.10	627.23	517.58	577.98	577.34	577.98	579.19	580.53
		P_{farm}	1156.28	1187.24	1429.60	1336.20	1211.57	1105.26	1165.66	1163.97	1236.33	1165.64	1165.51
8	0	P_I	$P_{arr} =$	490.36	490.43	490.63	490.98	491.37	491.71	491.97	492.15	492.24	492.12
		P_{II}	471.75	428.04	422.61	423.58	426.12	428.87	431.47	433.83	435.97	437.89	441.22
		P_{farm}	943.51	918.40	913.04	914.20	917.10	920.23	923.17	925.81	928.12	930.13	933.34
	22.5	P_I	$P_{arr} =$	496.79	497.85	499.28	500.21	500.77	501.11	501.32	501.45	501.49	501.37
		P_{II}	500.64	500.82	527.10	540.83	543.52	537.15	524.49	508.88	493.77	482.14	476.10
		P_{farm}	997.44	997.61	1024.95	1040.11	1043.73	1037.92	1025.60	1010.20	995.21	983.63	977.47
	45	P_I	$P_{arr} =$	498.77	499.54	496.58	498.10	500.37	497.98	496.65	499.21	499.62	497.41
		P_{II}	498.20	530.54	493.18	488.56	504.48	501.07	493.29	498.84	501.39	496.24	500.45
		P_{farm}	996.40	1029.31	992.71	985.13	1002.58	1001.44	991.27	995.49	1000.60	995.86	997.87
10	0	P_I	$P_{arr} =$	242.19	245.45	251.66	241.74	248.58	248.62	230.49	249.99	229.09	250.02
		P_{II}	246.53	223.10	223.00	224.68	226.38	227.39	228.66	231.27	230.19	224.88	232.07
		P_{farm}	493.07	465.28	468.45	476.34	468.11	475.97	477.28	461.76	480.18	453.98	482.09
	22.5	P_I	$P_{arr} =$	243.33	236.34	244.66	244.05	237.73	242.81	244.45	238.64	241.67	239.61
		P_{II}	241.63	240.30	247.39	253.12	257.67	259.23	228.66	258.52	230.19	251.79	242.77
		P_{farm}	483.26	483.64	483.73	497.79	501.72	496.96	471.47	502.97	468.83	493.46	482.39
	45	P_I	$P_{arr} =$	232.28	232.51	229.71	226.98	226.74	226.74	230.49	226.74	229.09	227.44
		P_{II}	228.83	243.37	235.01	223.53	222.60	230.10	230.10	231.27	230.10	224.88	233.25
		P_{farm}	457.66	475.65	467.52	453.24	449.58	456.84	456.84	461.76	456.84	453.98	460.69

8 s and finally T = 10. This is an expected trend given the behaviour of the disk-shaped buoy with resistive control that maximizes the motion close to the resonance period, T_r, of 4.6 seconds. Also note that in addition to the decrease in P_{farm}, $P_I + P_{II}$, with the wave period T, there is a slight decrease with increasing incidence angle β, especially for the case of T = 6 s. This is a consequence of the WEC arrays' shape, as seen in Fig. 2, where an increasing "shadowing effect" on the second row of devices for each WEC array is observed, as β increases toward 45°.

1) wave incidence at β = 0°: Results shown in Table I are displayed graphically in Fig. 5 for the three modelled wave periods to provide more insight into the data. In Fig. 5, we plot the power output for increasing separating distance D_1 between Arrays I and II for three incidence angles β= 0° (solid lines), β = 22.5° (dash-dot lines), and β = 45° (dashed lines). Figure 5(a) shows the result for T = 6 s, Fig. 5(b) for T = 8 s, and Fig. 5(c) for T = 10 s. Further, the thin horizontal lines represent the WEC farm power output as if the two arrays were to operate in isolation, that is 2 × P_{array}. The thick lines represent the total power output of the WEC farm, P_{farm}, where the two WEC arrays interact with each other. We can clearly notice the oscillating nature of the power output, with values both above and below the line showing case of arrays operating in isolation. Observe that the result for T = 6 s for β = 0° shows the greatest power oscillations. It should come as no surprise, seeing that in Fig. 4 (a) and (b) there is a strong rapidly oscillating pattern of $|\eta|$ in front of and in-between the WEC arrays. Note also that despite a single peak giving higher power output than the case of WEC arrays operating in isolation, the rest of the points fall well below this line. This clearly shows that the optimized staggered WEC array configuration results in substantial extraction of power from the incoming waves, and that when one WEC array is shadowing another, the effect is strongly negative. This deleterious effect of placing one WEC array in lee of another is mirrored in the results for T = 8 s (Fig. 5 (b)) and T = 10 s (Fig. 5 (c)). However, the power output results for T = 8 s do not show strong oscillations such as those observed for the other tested periods.

2) wave incidence at β = 22.5°: When a case is simulated where the incoming waves have an incidence angle β = 22.5°, we note a significant shift in the overall trends in the power output. First we point out that although for T = 6 s the power of the wave farm at β = 22.5° is generally lower than that for a head on wave (β = 0°), this is not true for T = 8 s and T = 10 s. For T = 8 s the power of twice both hydrodynamically

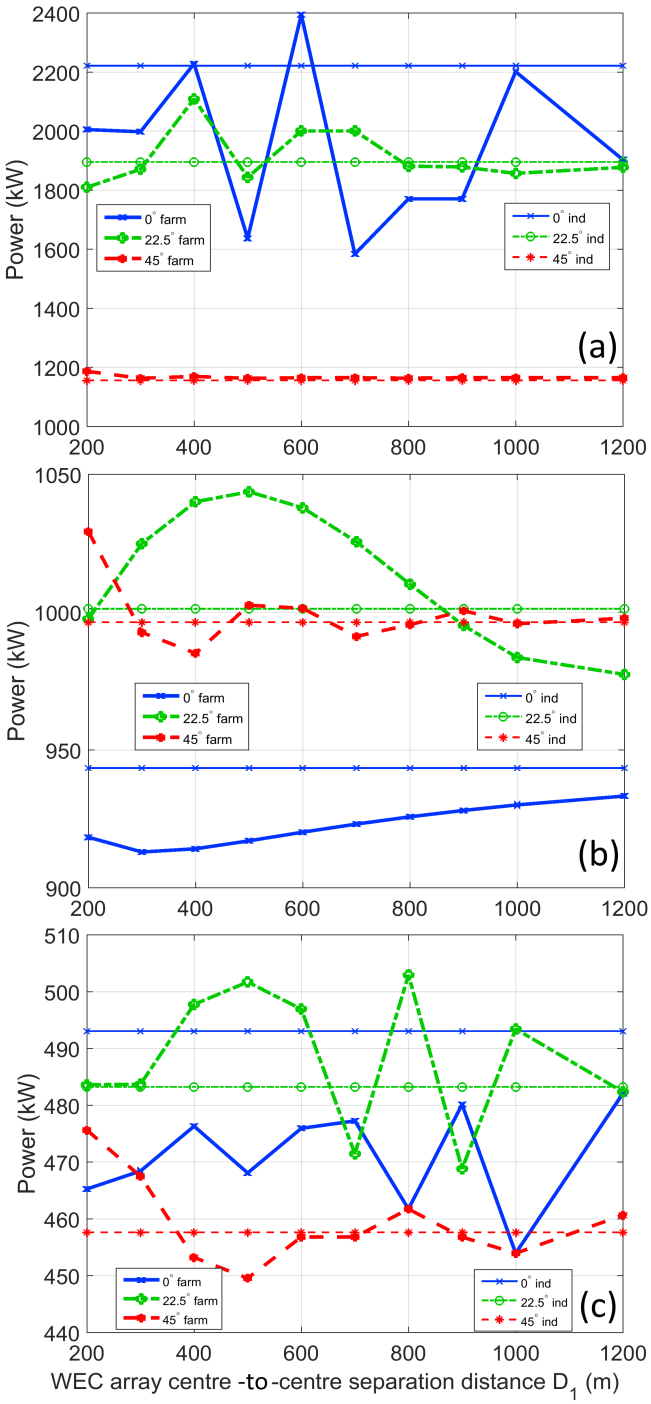

Fig. 5: POWER OUTPUT OF THE WEC FARM FOR VARIOUS INTER-ARRAY SEPARATION DISTANCES D_1 FOR REGULAR WAVE OF T = 6 s (a) T = 8 s (b) AND T = 10 s (c) FOR β = 0° (SOLID LINE), 22.5° (DASH-DOT LINE), AND 45° (DASHED LINE) THIN HORIZONTAL LINES INDICATE 2 × P_{array}. THICK LINES INDICATE P_{farm}

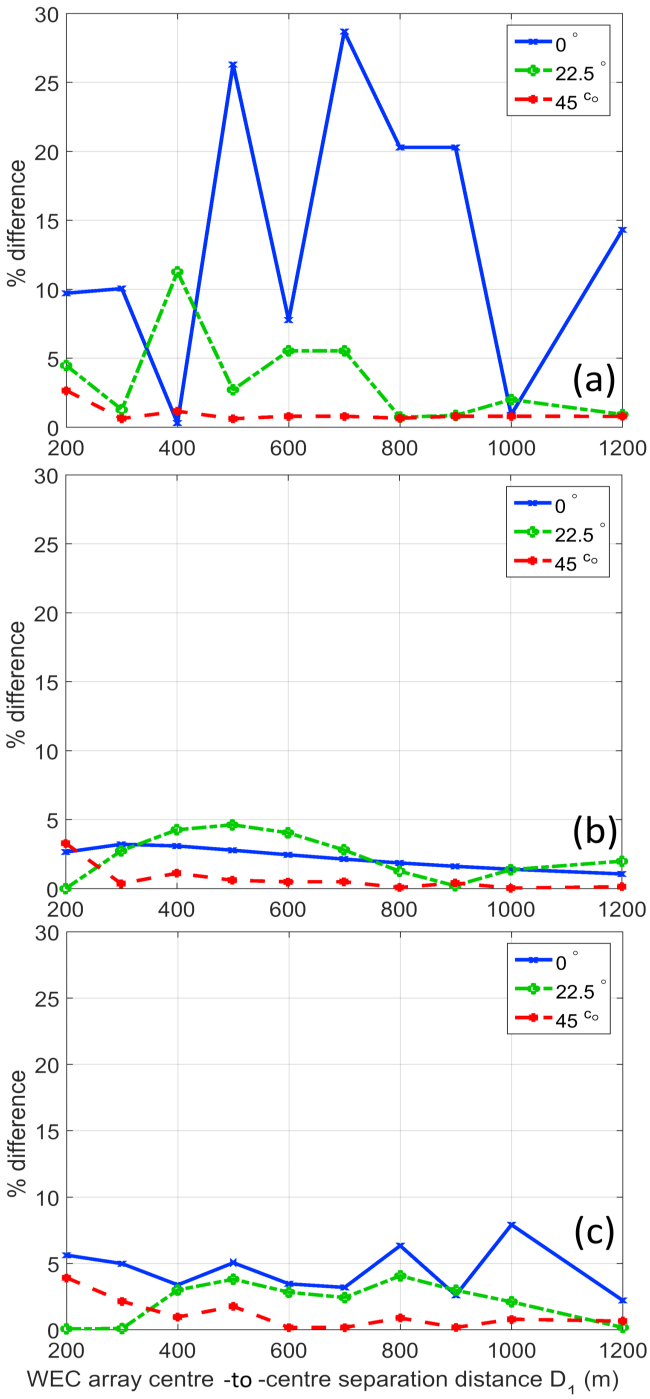

Fig. 6: PERCENT DIFFERENCE BETWEEN P_{farm} OF TWO WEC ARRAYS SEPARATED BY INTER-ARRAY DISTANCE D_1 AND 2 × P_{array} FOR REGULAR WAVE OF T = 6 s (a) T = 8 s (b) AND T = 10 s (c) FOR 0° (SOLID LINE), 22.5° (DASH-DOT LINE), AND 45° (DASHED LINE))

independent WEC arrays (P_{array}) and the wave farm (P_{farm}) is higher than for β = 0°. For T = 10 s, P_{farm} with β = 22.5 ° is lower than value of 2 × the hydrodynamically independent WEC arrays in head on waves but is higher than the result for P_{farm} with $|\beta|$=0°. We remark that the amplitude of the variability of the power output with respect to separation

TABLE II: PERCENTAGE DIFFERENCE (%) BETWEEN THE TOTAL POWER OUTPUT OF THE WEC FARM, P_{farm} (WEC ARRAYS INTERACT WITH EACH OTHER), AND THE POWER OUTPUT OF 2 $\times$ P_{array} (WEC ARRAYS ARE ISOLATED) FOR REGULAR WAVES WITH T = 6 s, T = 8 s, AND T = 10 s FOR FOR DIFFERENT WAVE INCIDENCE ANGLES, β

wave period T (s)	wave inc. angle β (°)	Separation distance, D_1, between WEC Array I and WEC Array II (m)									
		200	300	400	500	600	700	800	900	1000	1200
6	0	9.73	10.07	0.31	26.31	7.78	28.70	20.30	20.30	0.92	14.32
	22.5	4.49	1.28	11.28	2.72	5.56	5.56	0.74	0.87	2.02	0.94
	45	2.68	0.64	1.17	0.63	0.81	0.81	0.67	0.81	0.81	0.80
8	0	2.66	3.23	3.11	2.80	2.47	2.15	1.88	1.63	1.42	1.08
	22.5	0.02	2.76	4.28	4.64	4.06	2.82	1.28	0.22	1.38	2.00
	45	3.30	0.37	1.13	0.62	0.51	0.51	0.09	0.42	0.05	0.15
10	0	5.63	4.99	3.39	5.06	3.47	3.20	6.35	2.61	7.93	2.23
	22.5	0.08	0.10	3.01	3.82	2.84	2.44	4.08	2.99	2.11	0.18
	45	3.93	2.15	0.97	1.76	0.18	0.18	0.90	0.18	0.81	0.66

distance D_1 is roughly the same as for the case of head-on waves (or β = 0°).

3) wave incidence at β = 45 °: For the case of β = 45° we observe the inverse of the trends at β = 0°, with P_{farm} being substantially lower for T = 6 s and T = 10 s, and higher for T = 8 s. Again, this is a consequence of the staggered two row configuration of the WEC arrays in Fig. 2. In general, as the staggered configuration of the WECs becomes roughly aligned for the waves with β = 45°, there is significant "shadow effect" inside the WEC array, but not at the WEC farm level. This is why there is also less oscillation in the power output over the wave farm separation distances D_1. Note that for T = 8 s there is a slight difference in the behaviour of the power oscillations which is likely due to the effective wavelength being a multiple of the WEC row separation distance, d_x (Fig. 2).

V. Defining 'hydrodynamic independence' in a WEC Farm composed of 2 WEC Arrays

We have seen in Section IV-A that the various factors in play influencing the power output of a WEC farm lead to a very complicated pattern of interaction that can be hard to discern at times. It is natural then to ask how can we extract practical information from such data that can both serve to optimize the WEC farm layout for a specific goal, as well as to accurately calculate the wave fields around these agglomerations. For this reason we attempt to simplify the problem by quantifying the significance of the interactions by first setting the value of 5% as a 'significance' threshold. Consequently, we define a wave farm of two WEC arrays as "hydrodynamically independent" if the power output is within $\pm$ 5% of the power output by two independent WEC arrays that operate in isolation (the case of 2 $\times$ P_{array}). We recall here that in the hydrodynamically independent case the power output is computed for each WEC array separately. An undisturbed wave field is used as input for the equations of motion of the WEC array. The power output for the case where there is interaction between the WEC arrays is determined by the iterative procedure outlined in Section III-D where the input wave field is the sum of the incident and perturbed waves. To do so, we first need to reformulate the results outlined in Section IV-A in terms of the percentage difference between the hydrodynamically independent case and the fully coupled wave farm. In Table II we show the results of Section IV in terms of this percentage difference. For brevity, only the result for the total power of the wave farm, P_{farm}, corresponding to the third row for each case in Table I, is shown. Again, displayed in a graphical format in Fig. 6, the results are more intuitive. We show the percentage difference between the coupled wave farm, where the WEC arrays interact, and the two isolated WEC arrays in Fig. 6 for T = 6 s (a), T = 8 s (b), and T = 10 s (c), respectively. Note that unlike in Fig. 5, in Fig. 6 the vertical scale is the same. We immediately note that only for the case of T = 6 s and β = 0° the difference is greater than 10 % for a range of separation distances. For the rest of the cases investigated, the difference is small, and in fact for T = 10 s only the head-on waves result in a difference larger than 5%. For T = 8 s, for all three wave incidence angles, the % difference is below the "5% hydrodynamic independence" threshold. We can therefore conclude that apart from the T = 6 s case, where the frequency response is close to resonance (T_r = 4.6 s) for the simulated WEC, and for the 'worst' incidence angle of β = 0° which causes the highest "shadow effect" down-wave of the WEC array, calculating the power output of the wave farm (P_{farm}) as 2 $\times$ P_{array} will not lead to a gross error.

A. Factors that Influence the Hydrodynamic Independence of two WEC arrays

In Section V we saw that the separation distance between the WEC arrays in a WEC farm is not the only factor that plays a role in determining the extend to which two WEC arrays are hydrodynamically linked. It should be noted that the extent of the separation distance that we have modelled is

limited from a practical standpoint, and several studies [2], [21] show that in regular waves two devices can have an appreciable hydrodynamic influence on each other even when they are separated by more than 2 kilometre. However, we have chosen to limit the separation distance D_1 in our study for practical reasons: if we are to consider a wave farm as a unit it is highly unlikely that they will be separated by more than a km with no other devices in the interceding space. Yet even over the limited separation distance we have seen quite a variety of behaviour in the interaction strength, as manifested in the values of the wave farm power output (P_{farm}), over the different cases. Obviously the wave period has the strongest influence on the overall power output, observed in Fig. 6 as is expected for a narrow banded device like a heaving buoy. Yet normalized for the total power output, the difference between $2 \times P_{array}$ and P_{farm} is not so great away from the wave period that is closest to the T_r of the device. What is clearly demonstrated is the influence of the wave incidence angle on the power output results. Not only does the overall magnitude of the interaction effects decrease as the wave incidence changes from a β = 0° heading to a β = 45°, but the variability over the range of D_1 decreases as well. Again, this is a result of the relative position of the WEC arrays; when one array is not directly shadowing another, the likelihood of a decrease in the performance of WEC array located downwave is reduced. Consequently, the waves that interact with the WEC array located downwave is closer to the undisturbed incident wave and by extension the waves which interact with the WEC array located upwave. We should also remark an important point about the trends seen in Fig. 5, and in Table I. Particularly, a small subset of the WEC array interactions within the wave farm is beneficial, that is when the total power of the wave farm is greater than the sum of two interdependent WEC arrays ($2 \times P_{array}$). This is largely due to the WEC type and the limitations of the linear resistive PTO modelled. As is shown in a number of investigations, e.g. [19], [22], one needs to implement active frequency-dependent control in order to fully take advantage of WEC motions to induce beneficial hydrodynamic interactions between devices and by extension, between WEC arrays.

VI. DISCUSSION

An iterative coupling methodology between the near-field BEM solver and the far-field wave propagation model introduced in [13] and [15] is applied in this paper. It provides a robust method for calculating the wave field around compact arrays of WECs and in turn allows us to estimate the total power output of a wave farm. However, although it provides accurate results to an arbitrary degree of precision, even a few orders of interactions require a complicated web of iterations as explained in Section III-D. Hence, it is natural to investigate the need to apply the technique of Fig. 3 to calculate the perturbed wave field within a farm due to WEC array interaction in order to extract wave power. If we can assume that two WEC arrays (I and II) in a farm are hydrodynamically independent, then the power absorbed by each WEC array can simply be computed once. The total wave field in a farm then can be also calculated as the sum of two perturbed wave fields generated by WEC Array I and WEC Array II where the motion of both arrays is forced by the incident wave only. The observed response mirrors exactly the trend that has been demonstrated for individual devices placed at increasing distances from each other within WEC arrays of various configurations such as in [11], [21], [23]. In these studies the net power in a WEC array trends to the sum of the power of isolated WECs as the separation distance becomes larger. In our investigation, however, we are able to demonstrate the same trend, but this time for a WEC farm composed of WEC arrays. A similar conclusion was reached in [23], where the authors separated a WEC farm into two clusters of WECs, showing a significant 'shadow effect' downwave of one cluster of heaving buoy type WECs. The authors conclude that offsetting clusters of arrays so that one is not directly behind another is the best array layout design strategy. However, they employed a BEM solver to calculate all of the interactions simultaneously, an approach that has limits as the number of simulated devices increases. While we observe an overall decrease in the magnitude of the inter-array interactions as we increase the array separation distance, consistent with the $1/\sqrt{2}$ asymptotic trend defined in [21], there is a significant difference in the smoothness of this curve between the various tested wave periods and incidence angles, β. Moreover, as we have noted in Section V-A, for the resistive damping scheme modelled in this study, the sum of the power output by the 2 isolated WEC arrays that do not interact with each other is higher than that of a WEC farm composed of 2 WEC arrays which interact (a net negative effect). We should point out however, that this is mainly due to the choice of the configuration of the individual WEC arrays which are optimized for a certain incident wave direction. Thus, when placed one behind another, power output of the WEC farm decreases. A different configuration for the WEC arrays, or indeed a different PTO model would likely have resulted in a different outcome.

VII. CONCLUSION

In this paper we have investigated the effect of separation distance on WEC farm power output using a novel coupling methodology. We have shown that for regular waves, for certain cases, two WEC arrays in a farm can be considered hydrodynamically independent for the purposes of assessing their impact on each other's power uptake. In this case a simple and fast coupling methodology can estimate the power production for the entire farm. In Section V we have investigated the magnitude of the error that is introduced into the calculation in making the assumption of hydrodynamic independence of the WEC arrays. We have demonstrated that for a majority of the tested regular wave conditions, the simplified approach of assuming WEC array hydrodynamic independence can be followed without losing appreciable accuracy in calculating the total WEC farm power. By presenting the results exhibited in Table I in the graphical format of Fig. 5 we have illustrated

the difference in the behaviour of the power output over different WEC array separation distances, for various wave incidence angles β and for different wave periods. We have seen that whilst the primary driver for the total power output of a WEC farm for a given wave height is the incident wave period, for a given wave period the impact of array interactions decreases with increasing separation distance. It should be mentioned that in this investigation we have focused on a narrow subset of modelling scenarios, namely that the study was performed for regular waves. Although we expect the overall trends in irregular waves to follow our observations in Section V and Section VI we make the following remarks. Firstly, the overall magnitude of the interactions between the WEC arrays will be decreased, as was shown for the case of individual devices in a WEC array in many other investigations. Therefore, although the computational cost to calculate the wave fields increases for multi-frequency irregular waves, the overall subset of cases that require the full computational hydrodynamically independent of Section III-D is much less than for regular waves. Hence we can calculate the majority of WEC farm layouts in realistic sea states using the simplified hydrodynamically 'independent' coupling technique. Our next steps are to demonstrate this result by extending the coupling hydrodynamically independent presented in this paper to realistic multi-frequency sea states.

ACKNOWLEDGEMENT

This research is being supported by the Research Foundation Flanders (FWO), Belgium - FWO.OPR.2.0 - FWO research project No. 3G029114.

REFERENCES

[1] C. Beels, P. Troch, G. D. Backer, M. Vantorre, and J. D. Rouck, "Numerical implementation and sensitivity analysis of a wave energy converter in a time-dependent mild-slope equation model," *Coastal Engineering*, vol. 57, no. 5, pp. 471 – 492, 2010.

[2] B. Borgarino, A. Babarit, and P. Ferrant, "Impact of the separating distance between interacting wave energy converters on the overall energy extraction of an array," in *Proceedings of the 9th European Wave and Tidal Energy Conference, Southampton, UK*, 2011.

[3] M. Göteman, J. Engström, M. Eriksson, and J. Isberg, "Optimizing wave energy parks with over 1000 interacting point-absorbers using an approximate analytical method," *International Journal of Marine Energy*, vol. 10, pp. 113 – 126, 2015.

[4] V. Stratigaki, P. Troch, T. Stallard, J. Forehand, D.and Kofoed, M. a. Folley, M. Benoit, A. Babarit, and J. Kirkegaard, "Wave basin experiments with large wave energy converter arrays to study interactions between the converters and effects on other users," *Energies*, vol. 7, pp. 701–734, 2014.

[5] V. Stratigaki, P. Troch, T. Stallard, D. Forehand, M. Folley, J. Kofoed, M. Benoit, A. Babarit, M. Vantorre, and J. Kirkegaard, "Sea-state modification and heaving float interaction factors from physical modelling of arrays of wave energy converters," *Journal of Renewable and Sustainable Energy*, vol. 7, no. 7, 2015.

[6] A. Babarit and G. Delhommeau, "Theoretical and numerical aspects of the open source bem solver NEMOH," in *Proc. of the 11th European Wave and Tidal Energy Conference 6-11th Sept 2015, Nantes, France*, 2015.

[7] P. Troch, "MILDwave - a numerical model for propagation and transformation of linear water waves." Department of Civil Engineering, Ghent University, Ghent. Internal Report., Tech. Rep., 1998.

[8] P. Troch and V. Stratigaki, "Phase-resolving wave propagation array models," in *Numerical Modelling of Wave Energy Converters*, M. Folley, Ed. Elsevier, 2016, ch. 10, pp. 191–216.

[9] M. Alves, "Wave energy converter modelling techniques based on linear hydrodynamic theory," in *Numerical Modelling of Wave Energy Converters*, M. Folley, Ed. Elsevier, 2016, ch. 1, pp. 11–65.

[10] A. Babarit, "On the park effect in arrays of oscillating wave energy converters," *Renewable Energy*, vol. 58, pp. 68–78, 2013.

[11] P. B. Garcia Rosa, G. Bacelli, and J. Ringwood, "Control-informed optimal layout for wave farms," *IEEE Transactions on Sustainable Energy*, vol. 6, pp. 575–582, 2015.

[12] A. Radder and M. Dingemans, "Canonical equations for almost periodic, weakly nonlinear gravity waves," *Wave Motion*, vol. 7, no. 7, pp. 473–485, 1985.

[13] V. Stratigaki, "Experimental study and numerical modelling of intra-array interactions and extra-array effects of wave energy converter arrays," 2014.

[14] T. Verbrugghe, P. Troch, A. Kortenhaus, V. Stratigaki, and A. Engsig-Karup, "Development of a numerical modelling tool for combined near and far field wave transformations using a coupling of potential flow solvers," in *Proc. of the 2nd Int'l Conference on Renewable Energies Offshore 24 - 26 October 2016, Lisbon, Portugal*, 2016.

[15] P. Balitsky, G. Verao Fernandez, V. Stratigaki, and P. Troch, "Coupling methodology for modelling the near-field and far-field effects of a wave energy converter," in *Proceedings of the ASME 36th International Conference on Ocean, Offshore and Arctic Engineering (OMAE2017)*, 2017.

[16] M. Brorsen and J. Helm-Petersen, "On the reflection of short-crested waves in numerical models," in *Proc. of the 26th Int'l Conference on Coastal Engineering, Copenhagen*, 1998, pp. 394–407.

[17] National Renewable Energy Laboratory. (2017) Marine and hydrokinetic technology database. [Online]. Available: http://en.openei.org/wiki/Marine_and_Hydrokinetic_Technology_Database

[18] F. Charrayre, C. Peyrard, M. Benoit, and A. Babarit, "A coupled methodology for wave-body interactions at the scale of a farm of wave energy converters including irregular bathymetry," in *Proc. of the ASME 2014 33rd Int'l Conference on Ocean, Offshore and Arctic Engineering June 8-13, 2014, San Francisco, CA, USA*, 2014.

[19] B. Child and V. Venugopal, "Optimal configurations of wave energy devices," *Ocean Engineering*, vol. 37, pp. 1402–1417, 2010.

[20] B. Child, J. Cruz, and M. Livingstone, "The development of a tool for optimising of arrays of wave energy converters," in *Proceedings of the 9th European Wave 1 Tidal Energy Conference, Southampton, UK*, 2011.

[21] A. Babarit, "Impact of long separating distances on the energy production of two interacting wave-energy converters," *Ocean Engineering*, vol. 37, pp. 718–729, 2010.

[22] P. Balitsky, G. Bacelli, and J. Ringwood, "Control-influenced layout optimization of arrays of wave energy converters," in *ASME. International Conference on Offshore Mechanics and Arctic Engineering, Volume 9B: Ocean Renewable Energy*, 2014.

[23] B. Borgarino, A. Babarit, and P. Ferrant, "Impact of wave interaction effects on energy absorbtion in large arrays of wave energy converters," *Ocean Engineering*, vol. 41, p. 7988, 2012.